ELSEVIER

Tectonophysics 321 (2000) 279–296

TECTONOPHYSICS

www.elsevier.com/locate/tecto

Seismic anisotropy under extended crust: evidence from upper mantle xenoliths, Cima Volcanic Field, California

B. Soedjatmiko [a], N.I. Christensen [b,*]

[a] *Department of Earth and Atmospheric Sciences, Purdue University, West Lafayette, IN 47906, USA*
[b] *Department of Geology and Geophysics, University of Wisconsin, Madison, WI 53706, USA*

Received 23 August 1999; accepted for publication 26 January 2000

Abstract

A model of P-wave velocity anisotropy and shear-wave splitting for upper mantle under extended crust is derived from comparisons of seismic field measurements and observed xenolith anisotropies. Seismic velocity measurements and anisotropies calculated from petrofabric measurements of 15 upper mantle xenoliths from the Cima Volcanic Field, Eastern Mojave Desert, California show average maximum anisotropies of 6.9% for V_p and 4.5% for V_s. Xenolith compressional wave velocities corrected for upper mantle temperature and pressure agree well with field observations in the vicinity of the Cima Volcanic Field. The velocities calculated from the olivine fabrics suggest that upper mantle foliations beneath the region are horizontal, and lineations trend ENE. The fabrics are believed to originate from early Cenozoic extension in the area, which had the same trend as the lineations. The unusually high upper mantle temperatures in this region apparently have not significantly affected upper mantle fabrics.

Keywords: anisotropy; olivine; petrofabrics; upper mantle; velocity; xenolith

1. Introduction

Mantle seismic anisotropy, a product of tectonic deformation, records deformational history. It plays an important role in the study of upper mantle deformation due to its ability to resolve directional features which provide information on upper mantle structures. Since the first geophysical observations of continental upper mantle Pn anisotropy (Bamford, 1973, 1977; Fuchs, 1977) and shear-wave splitting (Ando et al., 1983; Ando, 1984), seismic anisotropy has become an important tool in the study of upper mantle processes. Much of our understanding about upper mantle structure and rheology has been credited to a wealth of seismic anisotropy data accumulated from around the world (e.g., Silver, 1996; Savage, 1999; Smith and Ekstrom, 1999).

In addition to seismic studies, much can be learned about upper mantle anisotropy by examining mantle-derived xenoliths which provide clues to upper mantle composition and properties (e.g., Babuska, 1977; Mainprice and Silver, 1993; Ji et al., 1994). Measured and calculated xenolith seismic properties offer powerful tools to estimate in situ magnitudes and orientations of seismic velocity and anisotropy in the upper mantle that

* Corresponding author. Fax: +1-608-262-0693.
E-mail address: chris@geology.wisc.edu (N.I. Christensen)

0040-1951/00/$ - see front matter
PII: S0040-1951(00)00070-6

Table 1
Previous studies of mantle xenolith anisotropies

Authors	Number of xenoliths	Region	V_p measured	V_s measured	Fabric analysis	Anisotropy calculated	Geophysical analysis
Christensen (1966)	2	Hawaii	Yes	Yes	No	No	No
Kumazawa and Andrew (1971)	21	Colorado Plateau	Yes	No	No	No	No
Matshushima (1972)	1	Japan	Yes	No	No	No	No
Babuska (1976)	12	Hawaii, Sierra Nevada, New Mexico	Yes	Yes	Yes	No	No
Peselnick et al. (1977)	2	Sierra Nevada	No	No	Yes	Yes	Incorporation with Pn velocities
O'Reilly et al. (1990)	4	Australia	Yes	No	No	No	No
Mainprice and Silver (1993)	5	South Africa	No	No	Yes	Yes	Incorporation with shear wave splitting
Ji et al. (1994)	13	Canadian Cordillera	No	No	Yes	Yes	Incorpoartion with shear wave splitting
Kern, et al. (1996)	4	Baikal, Russia	Yes	Yes	Yes	Yes	No
Ismail and Mainprice (1998)	15	South Africa	No	No	Yes[a]	Yes	No
This study	15	Eastern Mojave Desert, California	Yes	Yes	Yes	Yes	Incorporation with Pn and shear-wave splitting

[a] Fabric data are from previous studies, including Mainprice and Silver (1993).

can be used to constrain and calibrate geophysical observations. Previous studies of mantle xenolith seismic properties generally emphasize either laboratory measured velocities or calculated anisotropies from fabric analysis (Table 1). In this study, both methods are incorporated in order to investigate seismic anisotropies of upper mantle xenoliths from Cima Volcanic Field, southeastern California, and to interpret seismic refraction and teleseismic observations of anisotropy in the region.

2. Xenoliths

The xenoliths were collected from a volcanic pipe in the Cima Volcanic Field, eastern Mojave Desert, located ca. 40 km east of Baker, California (Fig. 1). This volcanic complex is characterized by numerous basaltic pipes, which often contain abundant xenoliths, of Cenozoic age. Although the volcanism has been recorded during the last 13 myr, the emplacements of Cima xenoliths are relatively recent, between 0.6 and 0.06 myr (Wilshire, 1990). This region is considered the extension of the Basin and Range province and exhibits geophysical features characteristic of an extended terrane (Zoback et al., 1981). Among the prominent features include a thin crust (Mooney and Weaver, 1989), high heat flow (Sass et al., 1981), a very reflective lower crust (Louie and Clayton, 1987), strong Moho reflections (Goodwin and Thompson, 1988), and low Pn velocities (McCarthy et al., 1987).

Common Cima xenoliths include granite, gabbro, pyroxenite and peridotite, with sizes ranging from 3 to 30 cm. Based on their compositions, these xenoliths have been assigned as lower crustal and upper mantle in origin (Wilshire et al., 1991). The mantle xenoliths are harzburgite and lherzolite. The crystallographic texture is mosaic, equigranular, with grain sizes between 0.5 and 0.8 mm. Based on multiple thin section analyses olivine generally constitutes >80% of the total volume (Table 2). Olivine compositions range from 88 to 92% forsterite (Fo_{88}–Fo_{92}) based on measurements of angles between optical axes and microprobe data. Orthopyroxene is generally present as elongated grains, ranging from 0.1 to 0.6 mm in size, and characterized by abundant exsolution lamel-

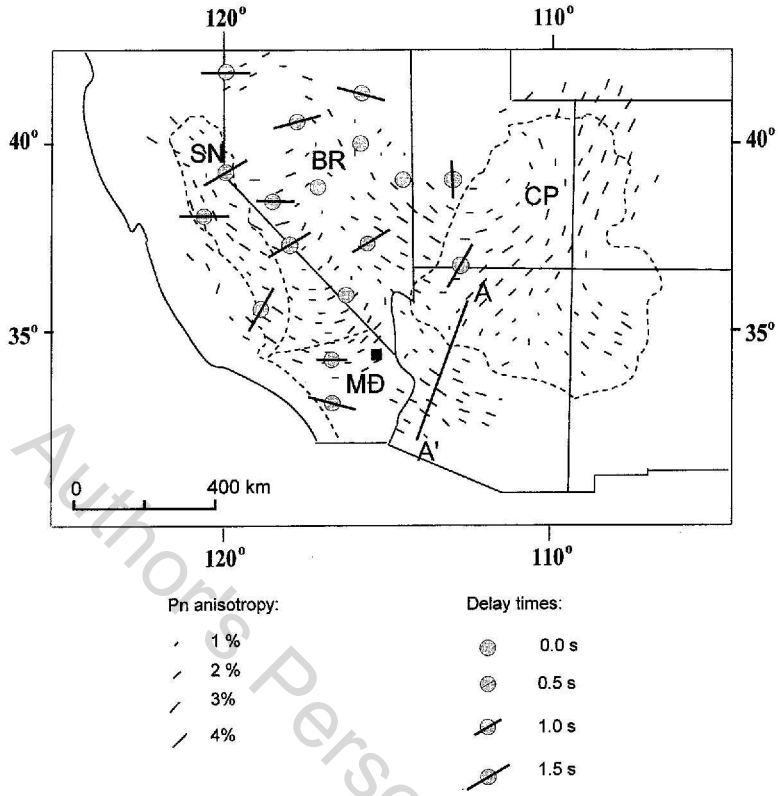

Fig. 1. Map of western United States showing geophysical features and the location of Cima Volcanic Field (■). Pn anisotropies are from Hearn (1996). Lines indicate fast Pn directions. Delay times are from Savage and Silver (1993), Ozalaybey and Savage (1995), and averages of clusters from Sheehan et al. (1997). ○, Locations of delay time observations, and the crossing line indicates fast vibration direction. A–A', Whipple Mountain seismic line (McCarthy et al., 1987). BR, Basin and Range; CP, Colorado Plateau; MD, Mojave Desert; SN, Sierra Nevada.

lae. Small amounts of spinel (<2%) are common in many xenoliths, and garnet is absent suggesting a shallow mantle origin. The xenoliths generally exhibit a grainy, sugary texture, and are commonly brittle. Many are bounded by multiple planar facets, resulting from upper mantle jointing (Wilshire and Kirby, 1989).

The original depths and temperatures of mantle xenoliths were estimated using single-pyroxene thermobarometry described by Mercier (1976, 1980). This method is based on theoretical derivations of equilibrium reactions between pyroxene (enstatite or diopside) and aluminous phases (spinel or garnet), and empirical relations between chromium content and aluminum solubility. It is applicable for a wide range of depths and tectonic environments, including continental extensions and cratons. The calculated errors are expected to be no greater than 3.0 MPa for pressure and 30°C for temperature (Mercier, 1980). It is found that the pyroxenes stabilized at temperatures between 955 and 1060°C and pressures between 0.9 and 1.4 GPa, which correspond to depths of 30–45 km. The pressures are slightly greater than estimates by Wilshire (1990) based on plagioclase–olivine stabilization, which suggested pressures of 0.8–1.1 GPa and temperatures of 885–1015°C.

3. Petrofabrics

Crystallographic preferred orientations were measured using a U-stage equipped with five independent axes, as described by Emmons (1943).

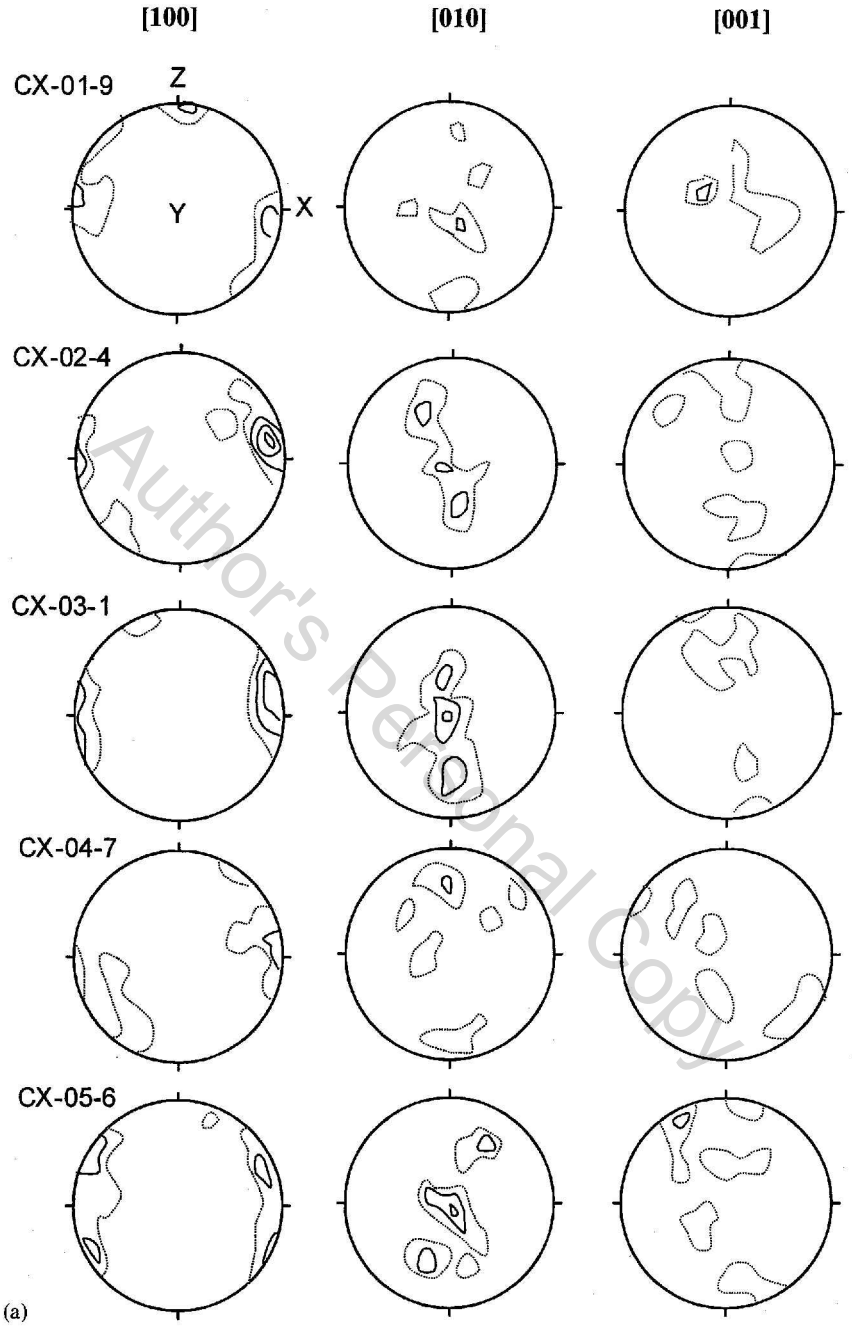

Fig. 2. (a) Olivine fabrics plotted on lower hemisphere projections. Fabrics are contoured at 2% intervals, with the lowest contours (2%) shown as dashed lines. X is lineation, and XY is foliation (parallel to page). (b) Orthopyroxene fabrics on lower hemisphere projections. Fabrics are contoured at 2% intervals, with the lowest contours (2%) shown as dashed lines. X is lineation and XY is foliation (parallel to page).

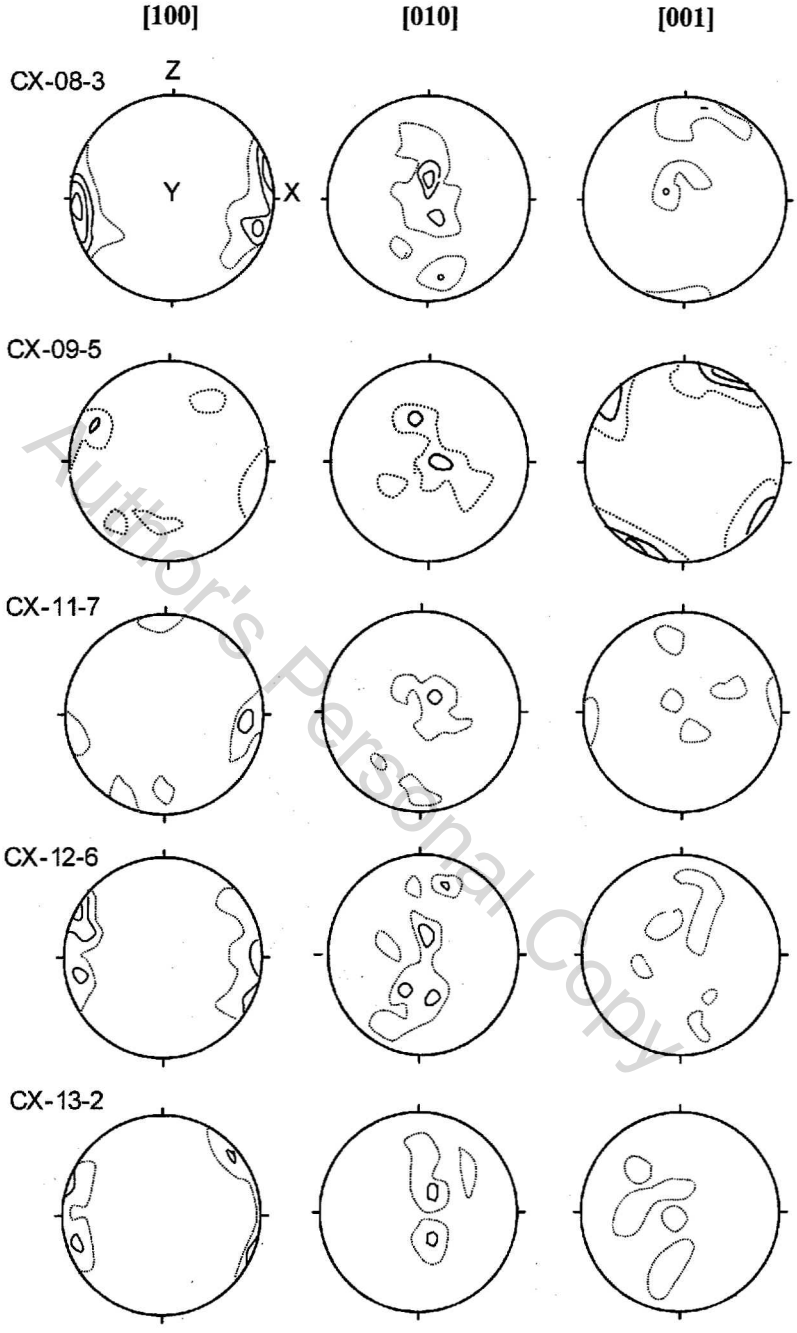

Fig. 2. (*continued*)

One or more thin sections were made from each xenolith, from which crystallographic orientations of olivine and pyroxene were measured. Between 100 and 150 olivine crystals were measured from each sample. Fig. 2a and b shows fabrics of each xenolith, plotted and contoured on lower hemi-

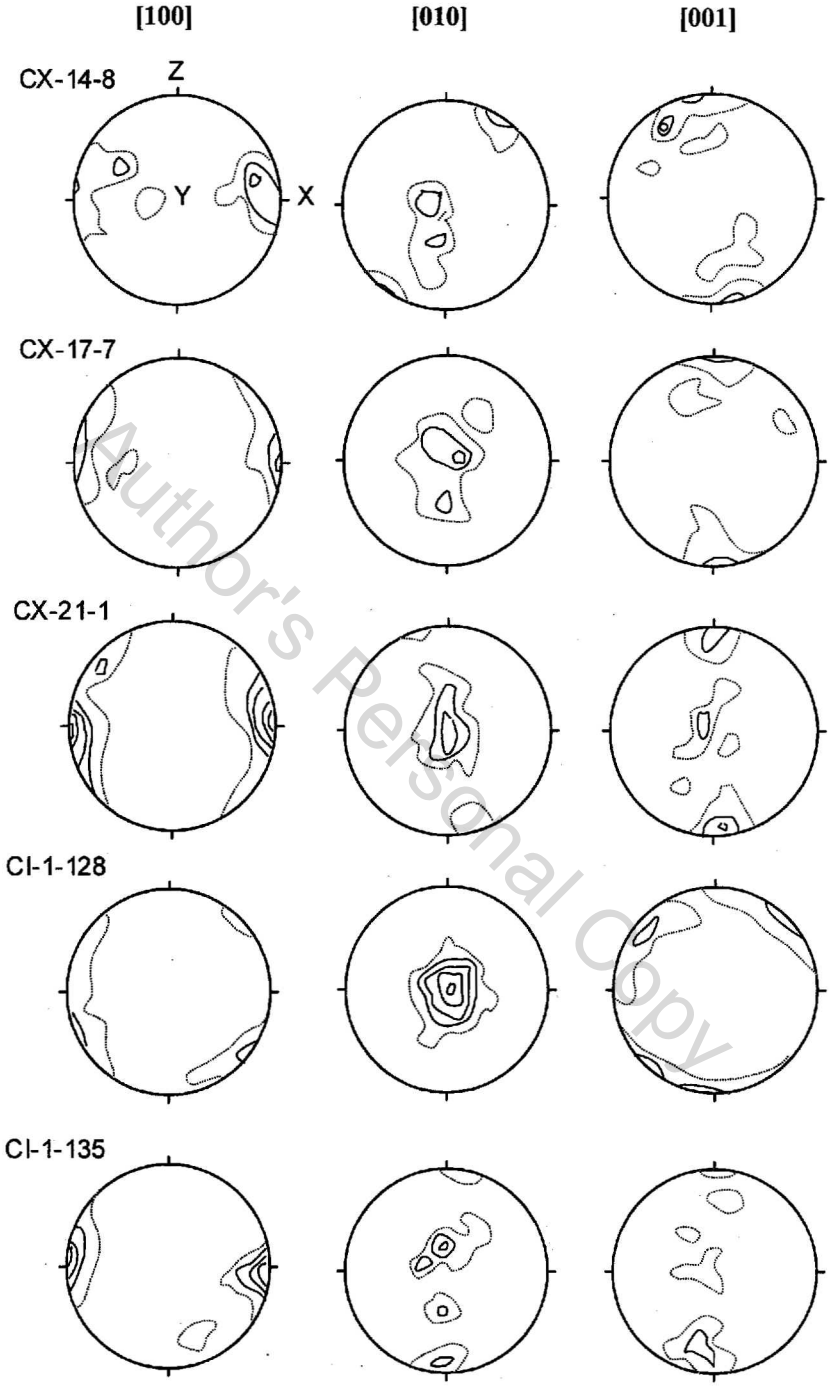

Fig. 2. (*continued*)

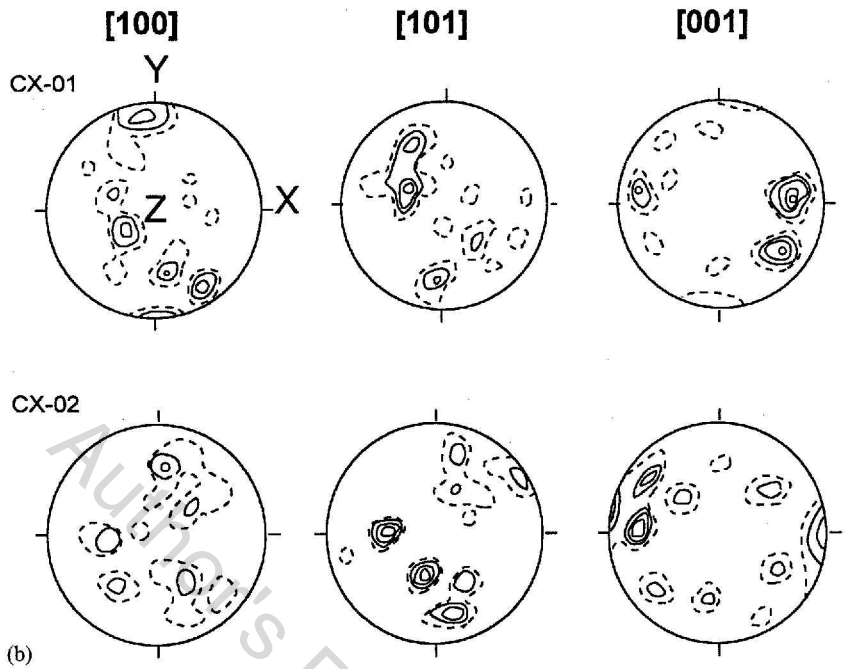

Fig. 2. (*continued*)

Table 2
Mineralogy of Cima xenoliths[a]

Sample	Density (kg m^{-3})	Ol (%)	Opx (%)	Cpx (%)	Sp (%)	Pl (%)	Measured velocity
CX-01-9	3250	78	19	2	1		$2V_p$
CX-02-4	3270	80	17	3	1		$1V_p$
CX-03-1	3220	54	38	7	1	<1	$1V_p$
CX-04-7	3110	82	17	1	<1		$1V_p$
CX-05-6	3140	70	27	3	<1		$1V_p$
CX-08-3	–	89	9	1	1		–
CX-09-5	–	93	6	1	–		–
CX-11-7	–	81	18	1	<1	<1	–
CX-12-6	3200	72	27	1	<1		$2V_p$
CX-13-2	–	68	31	2	1		–
CX-14-8	–	80	17	2	<1	<1	–
CX-17-7	3190	86	11	2	1		$1V_p$
CX-21-1	–	93	7	–	<1		–
CI-1-135	–	68	30	1	1	<1	–
CI-1-281	–	73	20	7	–		–

[a] Ol, Olivine; Opx, orthopyroxene; Cpx, clinopyroxene; Sp, spinel; Pl, plagioclase.

sphere projections. The reference direction X is lineation, Z is the foliation normal, and Y is an axis within the foliation plane, normal to X and Z. Foliations and lineations were recorded from hand specimen and microscopic observations (e.g., elongated spinels). The foliation (XY) planes are horizontal (parallel to the paper plane).

Olivine exhibits strong preferred orientations in all samples (Fig. 2a). Maxima of olivine a-axes, [100], are consistently parallel to lineations,

whereas olivine *b*-axes, [010], exhibit two different modes of population. In the first, *b*-axes form a strong maxima along the *Z*-axes, normal to foliations (e.g., CI-1-128). The second population, and the most common, has olivine *b*-axes girdles in the *YZ* planes, normal to lineations (e.g., CX-03-1). Similar fabrics are also observed in ophiolite peridotites of oceanic upper mantle origin (Christensen and Salisbury, 1979; Christensen, 1984) and in mantle xenoliths from the Canadian Cordilleras (Ji et al., 1994). Olivine *c*-axes, [001], fabrics show more variations. In most samples, the *c*-axes are scattered, lacking distinct orientation. In a few samples, *c*-axes fabrics show maximas along the *Y*-axes, normal to lineations (e.g., CX-17-7). In others, where strong concentrations of olivine *b*-axes are observed, olivine *c*-axes tend to girdle in the *YZ* plane, normal to lineations (e.g., CX-21-1).

The similarities of fabrics in most xenoliths suggest that they have been deformed by a similar deformation mechanism prior to their transportation to the surface and probably originated from the same depth range beneath the Moho. Kink banding and strong olivine *a*-axes maxima indicate that deformation by gliding along slip systems is dominant (Ave'Lallemant, 1975). The olivine *b*-axes girdles suggest that deformation was mostly limited to gliding through slip planes parallel to the *a*-axes, commonly known as (0*kl*)[100], under low to moderate strain rates (Nicolas, 1986). The lack of strong olivine *b*-axes concentrations also suggests moderate operating temperatures, consistent with the geothermometry estimates (Ave'Lallemant, 1975).

Pyroxene fabrics measured for two samples (CX-01 and CX-02) are considerably weaker than that of olivine, as shown on Fig. 2b. The pyroxene *c*-axes are weakly oriented parallel to lineation in the foliation plane, parallel to the olivine *a*-axes, whereas the other two axes have no distinct orientation and generally scatter around the foliation plane.

The weak pyroxene fabrics are related to the higher rigidity of pyroxene crystals. For the mineral chemistry of our samples (Fo_{88}–Fo_{92} and En_{90}–En_{93}), orthopyroxene has stronger resolve shear stress than olivine, and therefore requires greater energy to deform (Wenk and Bennet, 1991). In addition, pyroxene makes up much less volume of the bulk composition. Because a small fraction of more rigid pyroxenes flow in a more ductile olivine matrix, a larger part of the strain is accommodated by the more ductile olivine mass. As a result, pyroxene crystals are protected from significant strain and are less prone to deformation.

4. Stress field geometry

Laboratory experiments and field observations indicate that olivine and pyroxene preferred orientations correlate to stress orientations and flow

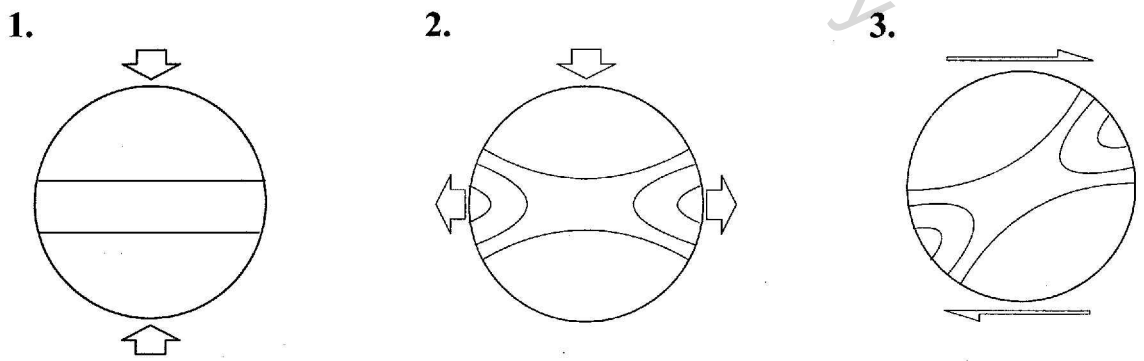

Fig. 3. Relations between deformation geometry and fabrics of olivine *a*-axes (after Ave'Lallemant, 1975; Takeshita et al., 1990; Wenk and Bennet, 1991). 1, Uniaxial stress with olivine *a*-axes spread out on a plane normal to maximum principal stress to produce transverse isotropy; 2, pure shear deformation with olivine *a*-axes concentrated parallel to the direction of minimum stress; 3, simple shear with olivine *a*-axes oblique to the shear plane. As the shearing proceeds, the *a*-axes will eventually parallel the shear plane.

geometry (e.g., Carter et al., 1972; Christensen, 1984). Of particular importance is the use of olivine preferred orientation to infer stress field geometry. Three types of commonly observed olivine preferred orientations are shown in Fig. 3, along with their associated deformational geometry: axial compression, pure shear (flow), and simple shear. In a dynamic upper mantle condition, rocks generally deform in either a pure shear or simple shear fashion (Takeshita et al., 1990).

Regardless of the deformational geometry, the relation between olivine fabrics and directions of principal stresses is generally simple and consistent, even though rock fabrics themselves are not a direct product of stress. Of particular importance is the behavior of olivine (010) planes and olivine *a*-axis. Olivine (010) planes have a tendency to rotate parallel to foliation planes (Ave'Lallemant, 1975), and as a result, olivine *b*-axes tend to align normal to foliations or parallel to the direction of maximum compression. Field observations in ophiolite tectonites and mylonitized dunite also indicate that olivine *b*-axes are generally normal to shear planes (Christensen, 1984). On the other hand, olivine *a*-axes tend to align parallel to the direction of minimum stress or maximum extension (e.g., Ave'Lallemant, 1975). Under uniaxial compression, in which maximum extension is laterally distributed on a plane normal to maximum compression, olivine *a*-axes tend to rotate normal to the direction of compression to produce lateral isotropy. Such orientation, however, is rarely observed in upper mantle xenoliths, because uniaxial compression is absent or minimal.

Under flow deformation (or pure shear) the olivine *a*-axes tend to rotate toward the direction of flow (or minimum stress), which generally coincides with lineation, and under simple shear deformation, olivine *a*-axes are oriented at oblique angles to the shear planes (Fig. 3). This obliquity, however, is non-unique and could change depending on the duration and the degree of shearing. With prolonged shearing, the *a*-axes further rotate toward the shear plane and eventually will be parallel (Takeshita et al., 1990). The actual angles between olivine *a*-axes and foliation planes can be directly observed in thin sections cut normal to foliation. In Cima xenoliths they range between 1 and 18°, with the majority falling within the 5–10° range, or almost parallel to foliation planes. Based on experimental results of Zhang and Karato (1995) this indicates strain in excess of 150%. For simplicity, throughout this study it is assumed that the olivine *a*-axes are concentrated in the foliation planes, and the *b*-axes are normal to foliation and lineation.

Recent forward modeling of the development of olivine fabrics for different deformational regimes in the lithospheric mantle (Tommasi et al., 1999) provides new information on expected anisotropy patterns for Pn and SKS observations. The modeling results predict strong anisotropy for both P and S waves in extensional regimes with fast P wave velocities approximately parallel to lineation, similar to our observations in Cima xenoliths. Tommasi et al. (1999) conclude that lithospheric extension and continental rifting produce fast Pn velocities and S-wave polarization directions oblique to the rift trend, because most rift systems undergo strike–slip motion as well as extension.

Pyroxene preferred orientations also provide valuable information about stress geometry. Orthopyroxene *c*-axes generally are concentrated in the foliation and parallel to lineation, similar to olivine *a*-axes orientations. [010] *b*-axes are also weakly concentrated in the foliation planes, but are normal to lineation. This preferred orientation is commonly observed in peridotites from ophiolite complexes (e.g., Christensen, 1984).

5. Seismic properties

Seismic properties of the xenoliths were determined using two methods. The first is a calculation based on the rock fabrics. These calculations commonly use orientation data from fabric analysis of 100 grains, and the results represent seismic properties of ideal samples, free of cracks, alteration and secondary minerals. The second method uses experimental laboratory velocity measurements at elevated pressures. This technique, which samples a much larger number of grains, gives the real seismic properties of rocks, resulting from all physical properties of the rocks, including accessory minerals, such as spinel.

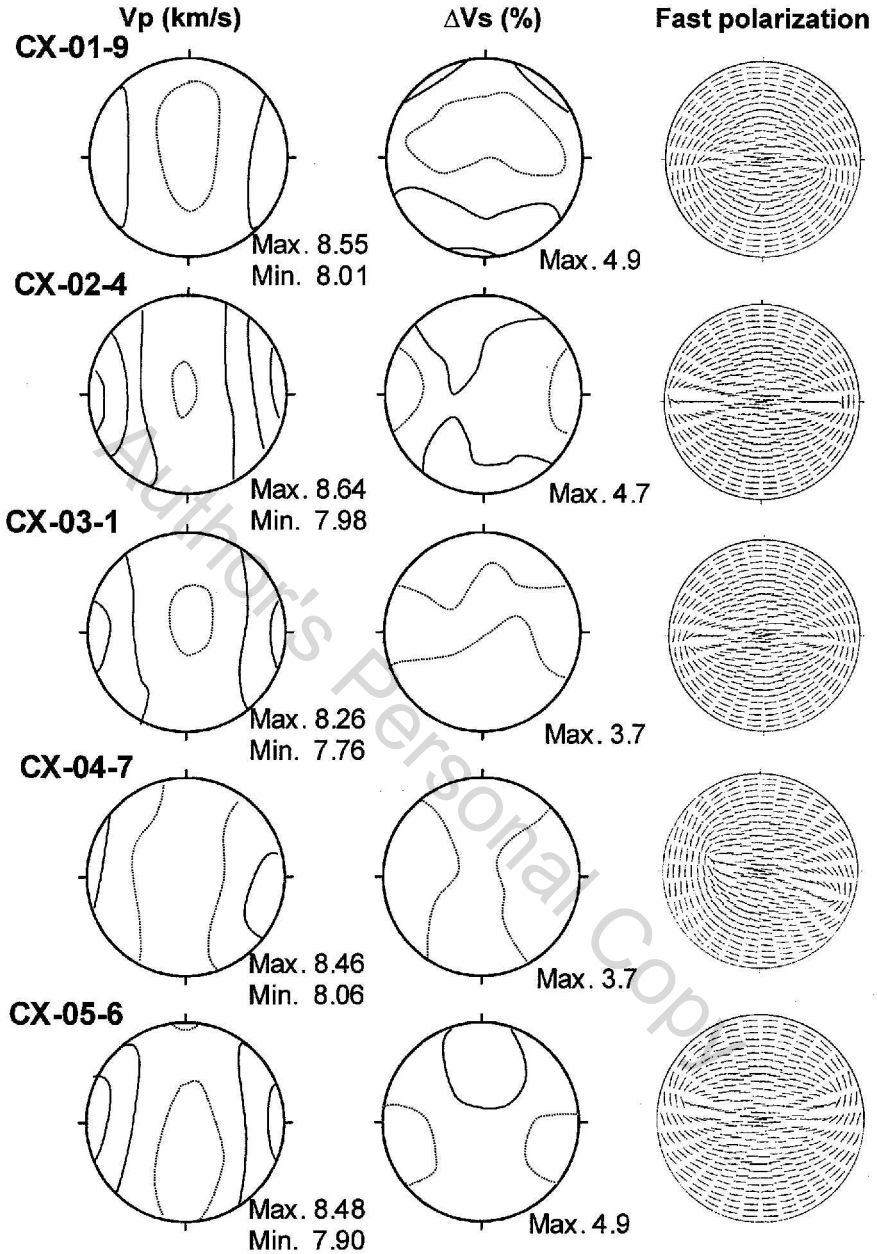

Fig. 4. Compressional velocity (km s^{-1}), shear-wave anisotropy (%) and vibration directions of the fast shear wave plotted on lower hemisphere projections. Contour intervals are 0.2 km s^{-1} for V_p and 2% for shear-wave anisotropy. Minimum contours are shown as dashed lines.

5.1. Velocity calculations

The use of mathematical computations to estimate xenolith seismic properties has advantages over laboratory measurements when xenoliths are small, and multiple cores are required for the laboratory measured velocities. Even if the size permits, xenoliths are often brittle and fractured,

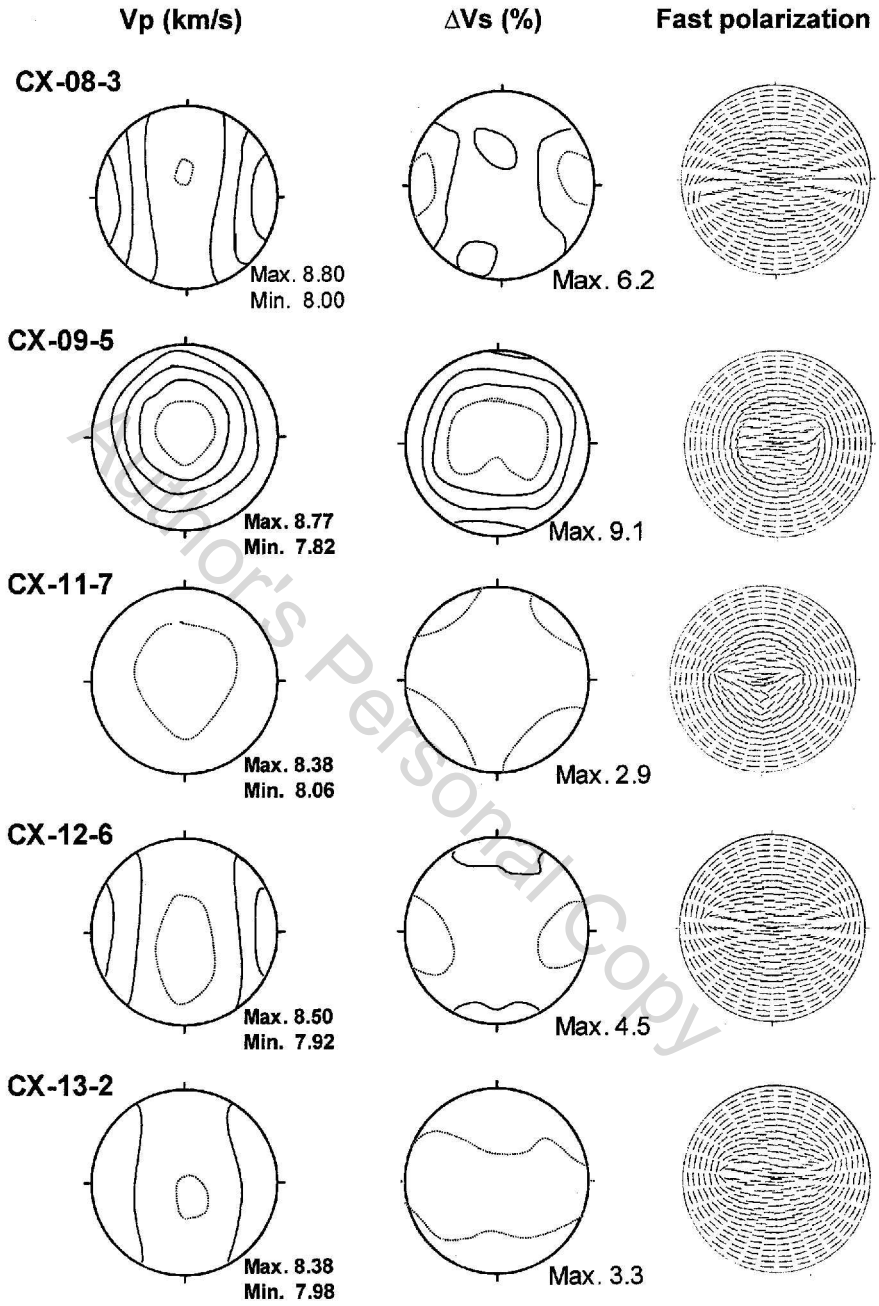

Fig. 4. (*continued*)

which make them difficult to core. In addition, complete P- and S-wave velocity surfaces can be calculated, whereas experimental measurements are usually performed in a few selected directions. The results can also be extrapolated to designated elevated pressures and temperatures of interest, using the data of Frisilio and Barsch (1972) and Kumazawa and Anderson (1971). The calculated

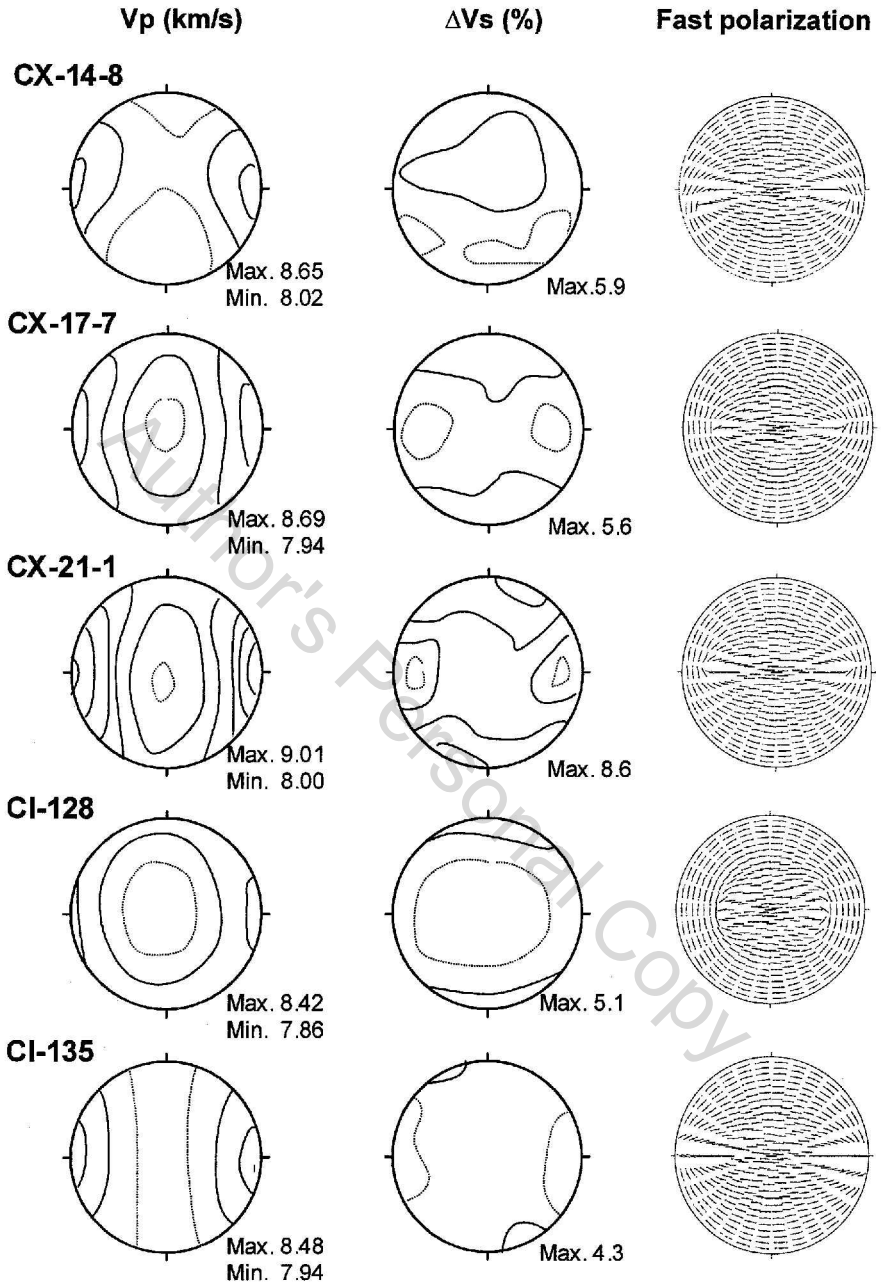

Fig. 4. (*continued*)

velocities generally agree with experimental results as was first demonstrated by Crosson and Lin (1971).

The properties of upper mantle xenoliths are controlled by a number of lithologic and physical factors, including fabrics, composition, confining pressure and temperature. All these factors are taken into account in the calculations of seismic

properties. For the purpose of these calculations, the xenolith compositions have been simplified to olivine and pyroxene because they are the major constituents. The calculations also require data of volume fraction, density and the elastic constants of the constituent minerals. The grain size is assumed to be uniform.

The seismic properties of the xenoliths were calculated using Christoffel equation:

$$\det|C_{ijkl}\ a_{ij} - \rho V^2 \delta_{ik}| = 0$$

where det is the determinant with respect to subscripts i and k; C_{ijkl} is the average elastic constants; a_{ij} is the direction cosines of the wave normal; ρ is the rock density; V is the phase velocity; and δ_{ik} is Kronecker's delta.

A numerical solution for the equation gives three unequal roots of V, which correspond to one quasi-longitudinal (compressional) and two quasi-transverse (shear) waves. A more detailed discussion of this method is given by Crosson and Lin (1971). In our calculations we used the Hill averaging method. The Voigt averaging technique (Crosson and Lin, 1971) gives slightly higher velocities, whereas recent experimental observations suggest that the shear-lag model, which gives lower velocities, may be more appropriate for olivine–orthopyroxene mixtures (Ji et al., 1994). For most averaging techniques calculated anisotropies are quite similar.

The calculated seismic velocities for each sample are shown in Fig. 4. The directional references are similar to those of Fig. 2, in which foliations are horizontal (parallel to the page). As can be seen in Figs. 2 and 4, the seismic properties are dependent on fabric strength and propagation direction. Xenoliths with strong fabrics exhibit higher anisotropies, and those with weaker fabrics exhibit lower anisotropies. In all xenoliths the maximum compressional velocities (V_p) are parallel to lineations (X), and the minimum are normal to foliations (Z). For calculations at a pressure of 1 GPa and room temperature, the magnitudes of maximum V_p range from 8.2 km s^{-1} to ca. 9.0 km s^{-1}, and of minimum range from 7.9 to 8.7 km s^{-1}. V_p anisotropies are generally consistent in all xenoliths, in which the greatest anisotropies are always observed for propagation in the XZ plane (normal to foliation and parallel to lineation), whereas the lowest V_p anisotropies are for propagation in the XY (foliation) plane. For shear-wave anisotropy, the delay time is maximum for propagation within the foliation planes and parallel to Y (normal to lineation), and minimum for propagation parallel to Z, normal to foliation (Fig. 4).

5.2. Laboratory measured velocities

Velocity measurements were conducted using an ultrasonic pulse transmission technique (Christensen, 1985) for samples of sufficient size for coring. Whenever possible, the cores were extracted at directions parallel to olivine a-axes maxima, which generally coincides with the direction of maximum V_p. Two samples (CX-01 and CX-12) were sufficient size to allow a second core parallel to b-axis maxima. Samples were cored with 2.54 cm diameters and lengths ranging from 2 to 3.5 cm. Both ends of the cores were polished to ensure a good contact between the core and the transducers. To prevent pressure fluid intrusion, the cores were jacketed with copper foil and then protected by a thick rubber tube before being inserted into the high pressure vessel for velocity measurements.

Measurements were performed at room temperature and pressures up to 600 MPa. The results are extrapolated to pressure of 1.0 GPa using a least square method to approximate the pressure at Moho depth. In the first 200 MPa, the observed V_p raises quickly, marking the closing of cracks and pore spaces within the xenoliths (Fig. 5). For low porosity (high density) samples, the velocity increase generally becomes linear at pressures above 300 MPa. The high density samples give seismic velocities which agree well with the calculated velocities. Fig. 5 shows that the calculated and measured velocities merge at pressure ca. 900 MPa, which is comparable to lithospheric pressure at around Moho depths. This also probably marks the pressure where all pores and openings in these samples are closed at room temperature.

In xenoliths with low densities, measured velocities are lower than calculated velocities (Fig. 6). Discrepancies between measured and calculated can be as high as 14%. The explanation for this

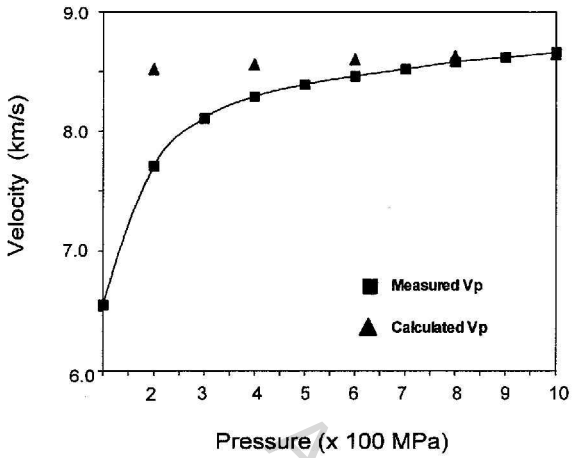

Fig. 5. Comparison between measured and calculated velocities for sample CX-01-9 for wave propagation parallel to olivine *a*-axis concentrations at room temperature as a function of pressure. Calculated and measured velocities merge at ~900 MPa.

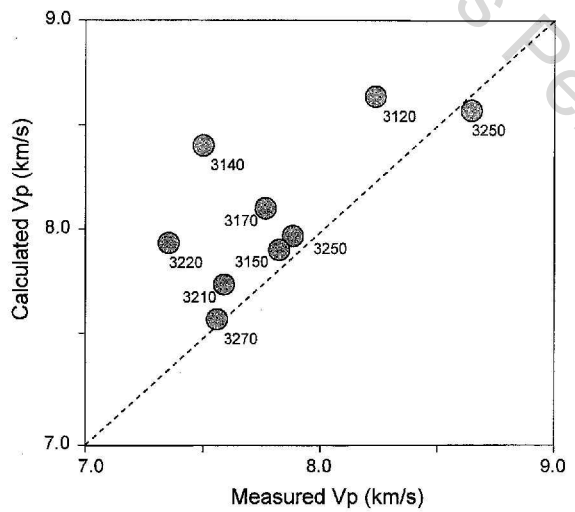

Fig. 6. Comparison of calculated and measured velocities at 1 GPa. Bulk densities in km m^{-3} are shown for each data set. Note the agreement between calculated and measured velocities for the high density rock cores. Samples with low densities have relatively high porosities and lower measured velocities than calculated velocities.

observation is higher porosity due to cracks which remain open at high pressures. The xenoliths were brought up to the surface by magmas at a very rapid fashion (Kushiro et al., 1976). During their ascent they were subjected to a rapid decrease in pressure, while the temperature remained high due to the entrapment by ascending magma. Rapid magma ascent is accompanied by rapid decompression that produces openings along grain boundaries and results in friable textures common to all Cima xenoliths. At the surface, the xenoliths were subjected to rapid cooling, which produced thermal cracking and further openings. These openings, which are caused by subsequent rapid decompression and cooling, cannot be completely closed during velocity measurements, even under high pressures up to 600 MPa. Kern et al. (1996) found that it requires pressures >600 MPa and temperatures >600°C to completely close crack openings in most xenoliths. In contrast, the emplacement history of ophiolites takes a more gradual path through tectonic processes. In ophiolite emplacement pressures and temperatures decrease very slowly and almost simultaneously, in which the effect of decompression and temperature drop tend to cancel each other. The formation of openings and cracks during tectonic emplacement is therefore relatively small or negligible, allowing better results in velocity measurements.

6. Discussion

Xenoliths brought up to the surface represent the geological conditions at their depth of origin at the time of emplacement. The emplacement of Cima xenoliths occurred between 0.6 and 0.06 Ma (Wilshire et al., 1991). Because their emplacement was recent, the xenoliths can be considered products of present day tectonics. Other than volcanism, the area has been tectonically inactive during the last several million years (Zoback et al., 1981). The xenolith's depth origin, which ranges between 30 and 36 km, is close to the 29 km Moho depth in the region (Mooney and Weaver, 1989). Because the xenoliths originate from about the same depth range as Pn velocities, they can be considered as representative of the upper mantle lid.

Observations from a seismic line, ca. 80 km to the south, give Pn velocities of 7.9–8.0 km s^{-1} and Moho depths of 29–33 km (McCarthy and Thompson, 1988; McCarthy et al., 1987). In the

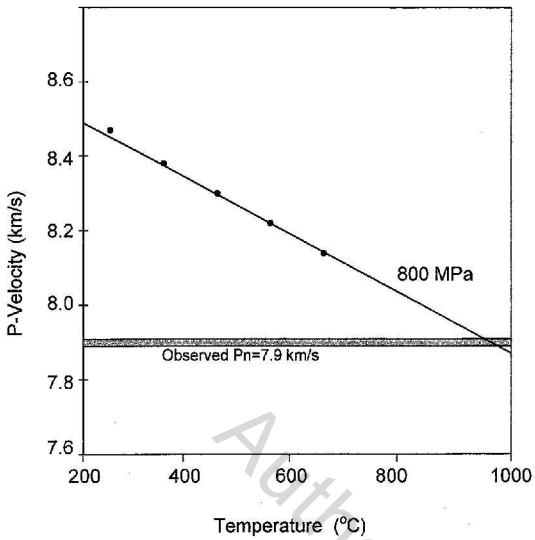

Fig. 7. Calculated maximum V_p of Cima xenoliths at estimated upper mantle pressures (800 MPa) as a function of temperature. The intersections between the calculated velocities and observed Pn velocities indicate a Moho temperature of 950°C.

vicinity of Cima Volcanic Field, Pn velocity is about the same at 7.9 km s^{-1} (Mooney and Weaver, 1989). Based on a depth of 29 km and average crustal density of 2800 km m^{-3}, the lithostatic pressure at Moho depth would be ca. 800 MPa. In order to compare seismic observations with xenolith data, seismic velocities of the xenoliths have been calculated for comparable pressures as a function of possible Moho temperatures. Fig. 7. shows that the calculated velocities agree with the observed Pn velocity at a temperature of ca. 950°C, which is consistent with thermal calculations by Lachenbruch and Sass (1978) for the Basin and Range province. Xenolith thermogeobarometry also indicates that the xenolith's parent rocks were formed at about the same temperature, suggesting that the xenoliths were detached directly from their parent rocks with very little time for cooling before reaching the surface.

Comparisons of the xenolith's properties and geophysical observations provide opportunities to reconstruct the original xenolith orientations in the mantle prior to their transportation to the surface and to deduce the attitudes of upper mantle structures. Two hypothetical conditions for horizontal lineation will be tested, that is, horizontal foliation and vertical foliation (Fig. 8). Pn velocity in this region agrees with calculated V_p for propagation parallel to lineation, suggesting that lineation in the upper mantle is horizontal. For horizontal foliation, the calculated compressional-wave anisotropy is 3.3%, and for vertical foliation the anisotropy is 6.9% (Fig. 8). Geophysical data in the vicinity of the Cima Volcanic Field, indicate a Pn anisotropy of 2.5–3% ($\sim$0.2 km s^{-1}), with maximum velocity trends to the east-northeast (Fig. 1). The magnitude of Pn anisotropy agrees well with the xenolith anisotropy for horizontal foliation. Vertical foliation produces unusually high anisotropy. Therefore, we conclude that the upper mantle foliations beneath Cima Volcanic Field are horizontal, and the direction of olivine *a*-axis maxima is ENE parallel to the maximum Pn velocity. This ENE orientation coincides with extension direction in that vicinity during early Cenozoic time (Zoback et al., 1981). If xenolith fabrics resulted from this early Cenozoic extension, it seems the fabrics have survived for >10 Ma, regardless of high upper mantle temperatures beneath the Basin and Range.

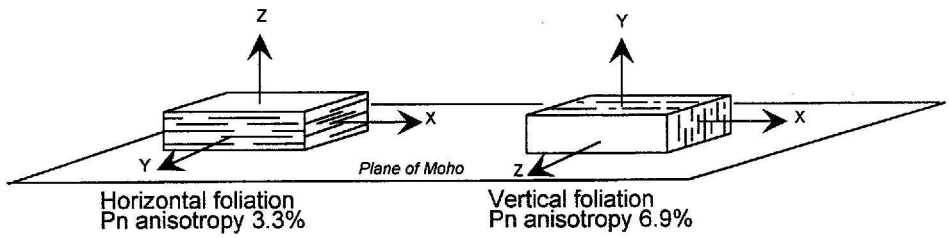

Fig. 8. Two possible orientations of upper mantle foliations in the vicinity of Cima Volcanic Field. *X*, Lineation, parallel to olivine *a*-axis maxima; *Z*, normal to lineation, parallel to olivine *b*-axis maxima; *Y*, normal to *X* and *Z*.

To the west of Cima Dome and in the central Mojave Desert, Pn velocities are maximum east-west, with anisotropies varying between 2.0 and 3.0% (Fig. 1). Shear-wave splitting observations ca. 90 km to the west of Cima Dome also show an east–west fast axis with a delay time of ca. 1.0 s (Liu et al., 1995; Ozalaybey and Savage, 1995b). The upper mantle thickness associated with this anisotropic slab is ca. 200 km based on seismic tomography (Hearn, 1996). These observations are consistent with calculated shear-wave splittings from xenoliths (2.3%), but the cause of the anisotropy is still uncertain. Ozalaybey and Savage (1995a) suggested that the east–west trend is caused by the 'frozen in' Farralon Plate which was subducted from the west beneath the region. Others argued that the trend is a result of recent contractions in southern California (Bartley et al., 1990; Liu et al., 1995), based on evidence of north–south Cenozoic contractions in southern California documented by Humpreys and Hager (1990). The compression is thought to be responsible for the formation of east–west trending structures in the area. Humpreys and Clayton (1990) also found a curtain-like high velocity anomaly beneath the transverse ranges which is believed to be caused by the same north–south compression. All these observations are consistent with the stress map of Zoback and Zoback (1980), which indicates a north–south compression in the vicinity of Mojave Desert area.

Under a north–south contraction, however, mantle deformation is expected to produce vertically oriented foliation with an east–west lineation. In the vicinity of Cima, however, the foliations appear to be horizontal and the observed maximum Pn velocity is trending northeast, instead of east–west like the rest of the Mojave Desert. This suggests that the north-south contractions affected only the central and western Mojave Desert. Vertically oriented foliation is also expected to produce considerably higher Pn and ΔV_s anisotropies than those observed in the area. It appears that deformation associated with the north–south contraction is limited only to the crust. Thus the shear-wave splitting observations in central Mojave Desert are more likely caused by a deeper feature, for example, the frozen in Farralon Plate.

7. Conclusions

This paper has presented an interdisciplinary approach between rock physics and geophysical observations to study seismic anisotropy and deformation mechanisms in the subcontinental upper mantle of southern California. Measured and calculated xenolith properties provide a valuable tool to constrain and calibrate the interpretation of seismic and teleseismic data in the region. Tectonic implications of these analyses can be summarized as follows.

1. Fabrics of Cima xenoliths exhibit strong olivine preferred orientation. Olivine *a*-axes are concentrated parallel to lineations, and *b*-axis are either normal to foliation or girdle on a plane normal to foliations and lineations. The fabrics are similar in most xenoliths, suggesting that they are resulted from the same deformation mechanism and perhaps originate from the same depth range.

2. Fabrics from Cima xenoliths are comparable to those of ultramafic tectonites from ophiolite localities. It is possible that upper mantle deformation in continental extension and under ocean ridges share a common mechanism.

3. Calculated and measured velocities agree fairly well for xenoliths with low porosity. For others, the measured velocities are lower than calculated velocities due to cracks which are not completely closed during experimental measurements. These openings are believed to be the result of rapid decompression during xenolith ascent to the surface, followed by rapid cooling at the surface.

4. The xenolith seismic properties are in a good agreement with geophysical observations in the Cima region and provide a useful tool to interpret geophysical data. Comparisons of xenolith properties and seismic data suggest that Pn anisotropy of 2.5–3.0% can only be explained with horizontal foliations in the upper mantle, with lineations trending ENE. It is possible that the fabrics are remnants of early Cenozoic extension in that vicinity, which also had a similar trend.

Acknowledgements

This research was supported by National Science Foundation Continental Dynamics

Program Grant No. EAR-93-17522. The assistance of K. Schram in petrofabric measurements and M. Savage, S. Ji and H. Durrast for constructive comments on the manuscript are greatly appreciated. H. Wilshire, G. Thompson and T. Parsons provided valuable help in collecting the xenoliths.

References

Ando, M., 1984. ScS polarization anisotropy around the Pacific Ocean. J. Phys. Earth 32, 179–195.

Ando, M., Ishikawa, Y., Yamazaki, F., 1983. Shear-wave polarization anisotropy in the upper mantle beneath Honshu, Japan. J. Geophys. Res. 88, 5850–5864.

Ave'Lallemant, A., 1975. Mechanism of preferred orientations of olivine in tectonite peridotites. Geology 3, 653–656.

Babuska, V., 1977. Elastic properties of ultrabasic xenoliths at pressures of up to 10 Kb. Phys. Solid Earth 13, 366–372.

Bamford, D., 1973. Refraction data in western Germany. J. Geophys. 39, 907–927.

Bamford, D., 1977. Pn Anisotropy in a continental upper mantle. Geophys. J. R. Astr. Soc. 49, 29–48.

Bartley, J.M., Glazner, A.F., Schermer, E.R., 1990. North–south contraction of the Mojave block and strike–slip tectonics in southern California. Science 248, 1398–1401.

Carter, N.L., Baker, D.W., George, R.P., 1972. Seismic anisotropy flow and constitution of the upper mantle. In: Heard, H.C., Borg, I.Y., Carter, N.L., Raleigh, C.B. (Eds.), Flow and Fracture of Rocks. Geophys. Monogr. Ser. AGU, Washington DC, pp. 167–190.

Christensen, N.I., 1966. Elasticity of ultrabasic rocks. J. Geophys. Res. 71, 5921–5931.

Christensen, N.I., 1984. The magnitude, symmetry and origin of upper mantle anisotropy based on fabric analyses of ultramafic tectonites. Geophys. J.R. Astron. Soc. 76, 89–111.

Christensen, N.I., 1985. Measurement of dynamic properties of rock at elevated temperatures and pressures. In: ASTM STP 869. American Society of Testing and Materials, Philadelphia, pp. 93–107.

Christensen, N.I., Salisbury, M.H., 1979. Seismic anisotropy of the oceanic upper mantle: evidence from the Bay of Islands Ophiolite Complex. J. Geophys. Res. 84, 4601–4610.

Crosson, R.S., Lin, J.W., 1971. Voigt and Reuss prediction of anisotropic elasticity of dunite. J. Geophys. Res. 76, 570–578.

Emmons, R.C., 1943. The Universal Stage, New York. Geol. Soc. Am. Mem. 8.

Frisilio, A.L., Barsch, G.R., 1972. Measurements of single-crystal elastic constants of bronzite as a function of pressure and temperature. J. Geophys. Res. 77, 6360–6384.

Fuchs, K., 1977. Seismic anisotropy of the subcrustal lithosphere as evidence for dynamical processes in the upper mantle. Geophys. J. R. Astron. Soc. 49, 167–179.

Goodwin, E.B., Thompson, G.A., 1988. The seismically reflective crust beneathhighly extended terrannes: evidence for its origin in extension. Geol. Soc. Am. Bull. 100, 1616–1626.

Hearn, T., 1996. Anisotropic Pn tomography in the Western US. J. Geophys. Res. 101, 8403–8414.

Humpreys, E.D., Clayton, R.W., 1990. Tomographic image of southern California mantle. J. Geophys. Res. 95, 19725–19746.

Humpreys, E.D., Hager, B.H., 1990. A kinematic model for the late Cenozoic development of southern California crust and upper mantle. J. Geophys. Res. 95, 19747–19762.

Ismail, W.B., Mainprice, D., 1998. An olivine fabric database: an overview of upper mantle fabrics and seismic anisotropy. Tectonophysics 296, 145–157.

Ji, S., Zhao, X., Francis, D., 1994. Calibration of shear-wave splitting in the subcontinental upper mantle beneath active orogenic belts using ultramafic xenoliths from the Canadian Cordillera and Alaska. Tectonophsics 239, 1–27.

Kern, H., Burlini, L., Ashchepkov, I.V., 1996. Fabric-related seismic anisotropy in upper-mantle xenoliths: Evidence from measurements and calculations. Phys. Earth Planet. Inter. 95, 195–209.

Kumazawa, M., Anderson, O.L., 1971. Elastic moduli, pressure derivatives and temperature derivatives of single crystal olivine and forsterite. J. Geophys. Res. 74, 5961–5972.

Kushiro, I., Yoder, H.S., Mysen, B.O., 1976. Viscosities of basalt and andesite melts at high pressures. J. Geophys. Res. 81, 6351–6356.

Lachenbruch, A.H., Sass, J.H., 1978. Models of an extending lithosphere and heat flow in Basin and Range province. In: Smith, R.B., Eaton, G.P. (Eds.), Cenozoic Tectonics and Regional Geophysics of Western Cordillera, Mem. Geol. Soc. Am. 152, 209–250.

Liu, H., Davis, P.M., Gao, S., 1995. SKS splitting in southern California. Geophys. Res. Lett. 22, 767–770.

Louie, J.N., Clayton, R.W., 1987. The nature of deep crustal structure in the Mojave Desert, California. Geophys. J. R. Astron. Soc. 89, 125–132.

Mainprice, D., Silver, P.G., 1993. Interpretation of SKS-waves using samples from the subcontinental lithosphere. Phys. Earth Planet. Inter. 78, 257–280.

Matshushima, S., 1972. Compressional wave velocity in olivine nodules at high pressure and temperature. Phys. Earth 20, 187–195.

McCarthy, J., Fuis, G., Wulson, J., 1987. Crustal stucture of the Whipple Mountains, souteastern California: a refraction study across region of large continental extension. Geophys. R. J. Astron. Soc. 89, 119–124.

McCarthy, J., Thompson, G.A., 1988. Seismic imaging of extended crust with emphasis on the western United States. Geol. Soc. Am. Bull. 100, 1361–1374.

Mercier, J.C., 1976. Single-pyroxene geothermometry and geobarometry. Am. Mineral. 61, 603–615.

Mercier, J.C., 1980. Single-pyroxene thermobarometry. Tectonophysics 70, 1–37.

Mercier, J.C., Nicolas, A., 1975. Textures and fabrics of upper-

mantle peridotites as illustrated by xenoliths from basalts. J. Petrol. 16, 454–487.

Mooney, W.D., Weaver, C.S., 1989. Regional crustal structure and tectonics of the Pacific coastal states: California, Oregon, and Washington. In: Pakiser, L.C., Mooney, W.D. (Eds.), The Geophysical Framework of the Continental United States, Mem. Geol. Soc. Am. 172.

Nicolas, A., 1986. Structure and petrology of peridotites: clues to their dynamic environment. Rev. Geophys. 24, 875–895.

O'Reilly, S.Y., Jackson, I., Bezant, C., 1990. Equilibrium temperature and elastic wave velocities for upper mantle rocks from eastern Australia: implications for interpretation of seismological models. Tectonophysics 185, 67–82.

Ozalaybey, S., Savage, M.K., 1995a. Double-layer anisotropy resolved from S phases. Geophys. J. Int. 117, 653–664.

Ozalaybey, S., Savage, M.K., 1995b. Shear-wave splitting beneath the western United States in relation to Plate tectonics. J. Geophys. Res. 100, 18135–18149.

Peselnick, L., Lockwood, J.P., Stewart, R., 1977. Anisotropic elastic velocities of some upper mantle xenoliths underlying the Sierra Nevada batholith. J. Geophys. Res. 82, 2005–2010.

Sass, J.H., Blackwell, D.D., Chapman, D.S., Costain, J.K., Decker, E.R., Lawver, L.A., Swanberg, C.A., 1981. Heat flow of the crust of the United States. In: Touloukian, Y.S., Judd, W.R., Roy, R.F. (Eds.), Physical Properties of Rocks and Minerals. McGraw-Hill, New York, pp. 503–548.

Savage, M.K., 1999. Seismic anisotropy and mantle deformation: what have we learned from shear wave splitting? Rev. Geophys. 27, 64–106.

Savage, M.K., Silver, P.G., 1993. Mantle deformation and tectonics: constraint from seismic anisotropy in the western United States. Phys. Earth Planet. Inter. 78, 207–228.

Sheehan, A.F., Jones, C.H., Savage, M.K., Ozalaybey, S., Dueker, K.G., Scheider, J.M., Bartsch, J.E., 1997. Contrasting lithospheric structure between the Colorado Plateau and Great Basin: initial results from Colorado Plateau–Great Basin PASCAL experiment. Geophys. Res. Lett. 24, 2609–2612.

Silver, P.G., 1996. Seismic anisotropy beneath the Continent: probing the depth of geology. Ann. Rev. Earth Planet. Sci. 24, 385–432.

Smith, G.P., Ekstrom, G., 1999. A global study of Pn anisotropy beneath continents. J. Geophys. Res. 104, 963–980.

Takeshita, T., Wenk, H.R., Milinari, A., Canova, G., 1990. Simulation of dislocation assisted plastic deformation in olivine polycrystals. In: Barber, D.J., Merediths, P.G. (Eds.), Deformation Processes in Minerals, Ceramics and Rocks. Unwin Hyman, London, pp. 365–377.

Tommasi, A., Tikoff, B., Vauchez, A., 1999. Upper mantle tectonics: three-dimensional deformation, olivine crystallographic fabrics and seismic properties. Earth Planet. Sci. Lett. 168, 173–186.

Wenk, H.R., Bennet, K., 1991. Modelling plastic deformation of peridotite with the self-consistent theory. J. Geophys. Res. 96, 8337–8349.

Wilshire, H.G., 1990. Lithology and evolution of the crust-mantle boundary region in the southwestern Basin and Range province. J. Geophys. Res. 95, 649–665.

Wilshire, H.G., Kirby, S.H., 1989. Dikes, joints, and faults in the upper mantle. Tectonophysics 161, 23–31.

Wilshire, H.G., McGuire, A.V., Noller, J.S., Turrin, B.D., 1991. Petrology of lower crustal and upper mantle xenoliths from the Cima volcanic field, California. J. Petrol. 32, 169–200.

Zhang, S., Karato, S., 1995. Lattice preferred orientation of olivine aggregates in simple shear. Nature 375, 774–777.

Zoback, M.L., Zoback, M., 1980. State of stress in the conterminous United States. J. Geophys. Res. 85, 6113–6156.

Zoback, M.L., Anderson, R.E., Thompson, G.A., 1981. Cainozoic evolution of the state of stress and style of tectonism of the Basin and Range province of the western United States. Philos. Trans. R. Soc. London 300, 407–434.